Bull. Chem. Soc. Jpn., **68**, 456—468(1995)

Headline Articles

Dinuclear Oxomolybdenum(V) and Oxotungsten(V) Complexes of the Hexadentate Ligands *N,N,N′,N′*-Tetrakis(2-pyridylmethyl)ethylenediamine and Its Propylenediamine Analog

Ryoichi Hazama, Keisuke Umakoshi, Akio Ichimura,† Shinji Ikari,†† Yoichi Sasaki,* and Tasuku Ito††

Department of Chemistry, Faculty of Science, Hokkaido University, Kita-ku, Sapporo 060

†Department of Chemistry, Faculty of Science, Osaka City University, Sugimoto, Sumiyoshi-ku, Osaka 558

††Department of Chemistry, Faculty of Science, Tohoku University, Aoba-ku, Sendai 980

(Received October 4, 1994)

Four new dinuclear oxomolybdenum(V) and oxotungsten(V) complexes, $[M_2O_2(\mu\text{-}O)_2(\mu\text{-tpen-}N,N')]^{2+}$ and $[M_2O_2(\mu\text{-}O)_2(\mu\text{-tppn-}N,N')]^{2+}$ (tpen=*N,N,N′,N′*-tetrakis(2-pyridylmethyl)ethylenediamine, tppn=*N,N,N′,N′*-tetrakis(2-pyridylmethyl)propylenediamine ((*R*)- and (*R,S*)-forms have been used); M=Mo, W), have been prepared. X-Ray structural analysis (except for the W–tppn complex) revealed 'basket type' structures similar to those of the edta and pdta analogs, $[M_2O_2(\mu\text{-}O)_2(\mu\text{-edta-}N,N'$ or $\mu\text{-pdta-}N,N')]^{2-}$ (edta=ethylenediamine-*N,N,N′,N′*-tetraacetate(4−); pdta=propylenediamine-*N,N,N′,N′*-tetraacetate(4−)). Crystal data are as follows. $[Mo_2O_2(\mu\text{-}O)_2(tpen)][MoCl_4O(H_2O)]Cl\cdot 2H_2O$ (**1a**): triclinic, space group $P\bar{1}$, a=13.686(3), b=14.783(3), c=9.650(3) Å, α=105.28(2), β=101.85(2), γ=76.27(2) °, V=1808.2(8) Å^3, and Z=2; $[Mo_2O_2, (\mu\text{-}O)_2(R,S\text{-tppn})](ClO_4)_2\cdot 2H_2O$ (**2**): monoclinic, space group $P2/a$, a=17.862(2), b=9.422(2), c=11.285(2) Å, β=106.65(1) °, V=1801.2(5) Å^3, and Z=2; $[W_2O_2(\mu\text{-}O)_2(tpen)](ClO_4)_2\cdot 2CH_3CN$ (**3**): triclinic, space group $P\bar{1}$, a=12.873(1), b=13.187(1), c=12.689(2) Å, α=97.80(1), β=116.08(1), γ=83.96(1)°, V=1914.3(4) Å^3, and Z=2. The metal–metal distances of the Mo–tpen, Mo–tppn, and W–tpen complexes are 2.546(1), 2.541(2), and 2.561(1) Å, respectively. Asymmetric distortion along the Mo–Mo axis of the Mo–*R*-tppn complex is in the opposite direction to that of the corresponding *R*-pdta complex. The difference may be related to the longer Mo–N(pyridyl) distance and larger N(pyridyl)–Mo–N(pyridyl) angle of the tppn complex as well as the direction of skew conformation of five membered chelate rings M–N(pyridyl)–C–C–N(amine). Electronic absorption spectral patterns of the new complexes are generally similar to the corresponding edta complexes. Circular dichroism (CD) spectra of the *R*-tppn complexes in the region >300 nm show a pattern nearly enantiomeric to those of the corresponding *R*-pdta complexes, indicating that the asymmetric distortion is retained in water and in acetonitrile. Kinetic parameters of the inversion of the pseudo-gauche conformation of diamine moiety in the tpen complexes were evaluated from the temperature dependence of ^{1}H NMR spectra in acetonitrile. $\Delta H^{\ddagger}$'s are significantly larger and $\Delta S^{\ddagger}$'s are significantly more positive than those of the edta analogs. The inversion may take place through dissociative bond cleavage of the metal–*N*(pyridyl) bond. The new dimolybdenum complexes show two reversible one electron reduction processes (at −1.40 and −1.86 V vs. Ag/Ag^+) in acetonitrile (0.1 mol dm^{-3}). Electronic absorption spectrum of the Mo_2(IV,V) mixed valence state was obtained using spectroelectrochemical techniques.

Most frequently encountered structures of d^1 oxomolybdenum(V) and oxotungsten(V) are dimers with the core $M_2O_2(\mu\text{-}E)_2^{(2+)}$ (M=Mo, W) with two oxide or sulfide bridges (E=O, S).[1—4] A metal–metal single bond is assumed to explain their diamagnetism and short metal–metal distances (2.5—2.85 Å).[1,2] A typical hexadentate ligand ethylenediamine-*N,N,N′,N′*-tetraacetate(4−) (edta) and its analog propylenediamine-*N,N,N′,N′*-tetraacetate(4−) (pdta) give $M_2O_2(\mu\text{-}E)_2^{(2+)}$ complexes with diamine moiety serv-

ing as an additional bridge.[5—12] Half of the ligand coordinates to each metal ion in the dimer. This unique structure may be called 'basket-type'. The basket-type structure is known for some other edta complexes of molybdenum such as a di-μ-hydroxo-μ-acetato molybdenum(III) dimer[13] and a tetramer of mixed-valence molybdenum(III,IV) complex.[14] Also $Mo_4(\mu_3\text{-}S)_4$-edta tetramers contain a part of the basket-type structure.[15—17] It should be noted, however, that these complexes are derived from $[Mo_2^{V}O_2(\mu\text{-}E)_2(\mu\text{-edta-}N,N')]^{2-}$. It appears that availability of just three facial sites of $Mo_2O_2(\mu\text{-}E)_2$ unit is critical to access to the basket type structure. With technetium(IV)[18] and rhenium(IV)[19] which also have a tendency to form edge-shared bioctahedron with a metal–metal bond, edta serves as tetradentate ligand to each metal ion in the $M_2(\mu\text{-}O)_2^{(4+)}$ dimer. In these cases four coordination sites are available for each metal ion in the dimer.

The ligand *N,N,N′,N′*-tetrakis(2-pyridylmethyl)ethylenediamine (tpen) has similar structure to edta, but carboxymethyl arms are replaced by 2-pyridylmethyl groups.[20] The tpen ligand gives a mononuclear seven coordinated species with rhenium(IV) rather than forming a di-μ-oxo dimer.[21] Interestingly, tpen but not edta provides basket-type complexes with vanadium(IV),[22] chromium(III),[23] and manganese(III,IV).[24] It is not appropriate to assume that edta and tpen form complexes with similar structure with a given metal ion.

Our initial purpose was to find if the hexadentate ligand tpen prefers to take a basket-type structure with oxomolybdenum(V) and oxotungsten(V). We have found tpen and its optically active derivative, *N,N,N′,N′*-tetrakis(2-pyridylmethyl)-(*R*)-propylenediamine (*R*-tppn), in fact give basket-type structures, $[M_2O_2(\mu\text{-}O)_2(\mu\text{-}L\text{-}N,N')]^{2+}$ (M = Mo, W; L = tpen, tppn). Some unexpected features were revealed as well as expected interesting redox properties. Asymmetric distortion along the Mo–Mo axis, which was found previously for the $[M_2O_2(\mu\text{-}O)_2((R)\text{-pdta})]^{2-}$,[11,25] has also been observed for the *R*-tppn analog, but surprisingly the direction is reversed, as revealed by structural and circular dichroism spectral results. Kinetic parameters of the pseudo-gauche ring inversion for the tpen complexes were also significantly different from those for the edta analogs.[11,26] Mixed-valence state, Mo_2(IV,V), of the tpen complex, has been characterized spectrophotometrically. This paper reports four new complexes of tpen and tppn and compares their various properties with those of the edta and pdta analogs.

Experimental

Materials. Ligands, *N,N,N′,N′*-tetrakis(2-pyridylmethyl)ethylenediamine (tpen), *N,N,N′,N′*-tetrakis(2-pyridylmethyl)-(*R*)-propylenediamine (*R*-tppn), and *N,N,N′,N′*-tetrakis(2-pyridylmethyl)-(*R,S*)-propylenediamine (*R,S*-tppn) were prepared by the reported methods.[27] Pyridinium salt of $[MoCl_5O]^{2-}$[28] and crude ammonium salt of the oxalato complex of tungsten(V)[29] were prepared as reported in the literature.

Di-μ-oxo-μ-[*N,N,N′,N′*-tetrakis(2-pyridylmethyl)-ethylenediamine-*N,N′*]-bis[oxomolybdenum(V)] Perchlorate, $[Mo_2O_2(\mu\text{-}O)_2(\mu\text{-tpen-}N,N')](ClO_4)_2$ (1): The ligand tpen (0.20 g, 0.48 mmol) was dissolved in a mixed solvent of CH_3OH (5 cm^3)–H_2O (15 cm^3) at 50 °C under an argon atmosphere. $(pyH)_2[MoCl_5O]$ (0.44 g, 0.99 mmol) was slowly added to the solution, which was then adjusted to pH 8 by adding aqueous 2 M (M=mol dm^{-3}) Na_2CO_3 solution slowly. After the filtration to remove precipitate, the filtrate was diluted with a large amount of water and passed through the column of SP-Sephadex C-25 cation exchanger. After the column was washed with water, an orange band was eluted with 1 M NaCl solution. The orange solution was concentrated and methanol was added to remove NaCl deposited by filtration. To the filtrate was added $NaClO_4$ (0.13 g, 0.96 mmol) in a small amount of methanol. Orange crystals were collected, washed with water and then ether, and dried in vacuo. Yield, 0.32 g (77%). Found: C, 35.04; H, 3.27; N, 9.30%. Calcd for $C_{26}H_{28}N_6O_{12}Cl_2Mo_2$: C, 35.51; H, 3.21; N, 9.56%. All the measurements for the complex cation $[Mo_2O_2(\mu\text{-}O)_2(tpen)]^{2+}$ except for the X-ray structural analysis were carried out with the perchlorate salt.

Di-μ-oxo-μ-[*N,N,N′,N′*-tetrakis(2-pyridylmethyl)ethylenediamine-*N,N′*]-bis[oxomolybdenum(V)] Chloride Aquatetrachlorooxomolybdate(V) Dihydrate, $[Mo_2O_2(\mu\text{-}O)_2(\mu\text{-tpen-}N,N')][MoCl_4O(H_2O)]Cl\cdot 2H_2O$ (1a): The ligand tpen (0.10 g, 0.24 mmol) and then $(pyH)_2[MoCl_5O]$ (0.22 g, 0.49 mmol) was added to acetonitrile (20 cm^3) under an argon atmosphere. While stirring, purple precipitate was deposited. This was removed by filtration. Dark purple crystals were obtained when the filtrate was allowed to stand. Found: C, 30.23; H, 3.40; N, 8.18%. Calcd for $C_{26}H_{34}N_6Cl_5Mo_3O_8$: C, 30.51; H, 3.35; N, 8.21%.

Di-μ-oxo-μ-[*N,N,N′,N′*-tetrakis(2-pyridylmethyl)-(*R,S*)-propylenediamine-*N,N′*]-bis[oxomolybdenum(V)] Perchlorate, $[Mo_2O_2(\mu\text{-}O)_2(\mu\text{-}R,S\text{-tppn-}N,N')](ClO_4)_2$ (2), Di-μ-oxo-μ-[*N,N,N′,N′*-tetrakis(2-pyridylmethyl)-(*R*)-propylenediamine-*N,N′*]-bis[oxomolybdenum(V)] Perchlorate, $[Mo_2O_2(\mu\text{-}O)_2(\mu\text{-}R\text{-tppn-}N,N')](ClO_4)_2$ (2R), and Di-μ-oxo-μ-[*N,N,N′,N′*-tetrakis(2-pyridylmethyl)-(*R*)-propylenediamine-*N,N′*]-bis[oxomolybdenum(V)] Hexafluorophosphate, $[Mo_2O_2(\mu\text{-}O)_2(\mu\text{-}R\text{-tppn-}N,N')](PF_6)_2$ (2Ra): The optically active complexes **2R** and **2Ra** were prepared by similar methods to that for **1** using *R*-tppn (0.20 g, 0.45 mmol) and $(pyH)_2[MoCl_5O]$ (0.22 g, 0.49 mmol). After NaCl was removed by filtration, $NaClO_4$ (0.13 g, 0.96 mmol) in a small amount of methanol was added to the filtrate to obtain **2R**. Yield, 0.23 g (57%). Found: C, 36.01; H, 3.57; N, 9.45%. Calcd for $C_{27}H_{30}N_6Cl_2Mo_2O_{12}$: C, 36.30; H, 3.39; N, 9.41%. The hexafluorophosphate salt **2Ra** was obtained by adding NH_4PF_6 instead of $NaClO_4$ to the filtrate. Found: C, 32.65; H, 3.10; N, 8.58%. Calcd for $C_{27}H_{30}N_6F_{12}Mo_2O_4P_2$: C, 32.94; H, 3.07; N, 8.54%. These salts were used for the spectrophotometric measurements.

The racemic complex **2** was prepared similarly by using recemic ligand *R,S*-tppn; it was used for X-ray structural analysis and NMR measurements. Found: C, 36.01; H,

3.37; N, 9.45%. Calcd for $C_{27}H_{30}N_6Cl_2Mo_2O_{12}$: C, 36.30; H, 3.39; N, 9.41%. A single crystal of **2** was obtained by diffusing ether into the acetonitrile solution.

Di-μ-oxo-μ-[*N,N,N′,N′*-tetrakis(2-pyridylmethyl)ethylenediamine-*N,N′*]-bis[oxotungsten(V)] Perchlorate $[W_2O_2(\mu\text{-}O)_2(\mu\text{-tpen-}N,N')](ClO_4)_2$ (3): To the suspension of tpen (0.29 g, 0.68 mmol) in water (10 cm^3) was added an aqueous solution (24 cm^3) of *p*-toluenesulfonic acid (0.52 g, 2.7 mmol) to dissolve tpen. Some crude ammonium salt of the oxalate complex of tungsten(V) (0.29 g, 0.45 mmol) was added to the solution at 50 °C under argon atmosphere. Calcium chloride dihydrate (0.20 g, 1.8 mmol) was then added to the solution and the resulting precipitate was removed by filtration. The pH of the filtrate was adjusted to 8 by slow addition of aqueous 2 M Na_2CO_3 solution at 50 °C under an argon atmosphere. Precipitate was removed by filtration at room temperature. The filtrate was diluted with a large amount of water and then passed through a column of SP-Sephadex C-25 cation exchanger. After the column was washed with water, a yellow band was eluted with 1 M NaCl solution. The orange solution was concentrated and methanol was added to remove NaCl deposited by filtration. To the filtrate was added $NaClO_4$ (0.13 g, 0.96 mmol). Yellow powder was collected, washed with ether, and dried in vacuo. Yield, 0.17 g (23%). Found: C, 28.34; H, 2.70; N, 7.46%. Calcd for $C_{26}H_{28}N_6Cl_2O_{12}W_2$: C, 29.60; H, 2.68; N, 7.97%. A single crystal for X-ray structural analysis was obtained by diffusing ether into the acetonitrile solution.

Di-μ-oxo-μ-[*N,N,N′,N′*-tetrakis(2-pyridylmethyl)-(*R*)-propylenediamine-*N,N′*]-bis[oxotungsten(V)] Perchlorate, $[W_2O_2(\mu\text{-}O)_2(\mu\text{-}R\text{-tppn-}N,N')](ClO_4)_2$ (4R): This was prepared by a method similar to that for **3**, using *R*-tppn (0.30 g, 0.68 mmol) and the crude ammonium salt of the oxalate complex of tungsten(V) (0.29 g, 0.45 mmol). Yield, 0.10 g (22%). Found: C, 29.05; H, 2.80; N, 7.78%. Calcd for $C_{27}H_{30}N_6Cl_2O_{12}W_2$: C, 30.33; H, 2.83; N, 7.86%.

Electrochemistry. Electrochemical measurements were performed at 25 °C in acetonitrile, which was dried over molecular sieves 4A and fractionally distilled, under an argon atmosphere, unless otherwise noted. The supporting electrolyte was tetrabutylammonium hexafluorophosphate (Bu_4NPF_6). This was prepared by metathesis of aqueous potassium hexafluorophosphate (Aldrich) and tetrabutylammonium bromide (Tokyo Chemical Industry) solutions, recrystallized three times from methanol, and dried at 70 °C under vacuum for 48 h before use.

Cyclic voltammetry at a glassy carbon disk electrode (3 mm diameter, Bioanalytical Systems) and steady state voltammetry at a carbon microdisk electrode (7 μm diameter, Bioanalytical Systems) were conducted with a Huso Electrochemical System HECS-972 microelectrode potentiostat and a Huso Electrochemical System HECS-321B potential sweeper. The electrodes were successively polished with 0.3 and 0.06 μm alumina and rinsed thoroughly with water and acetone. The voltammetric data were digitized and stored in an NEC PC9801 personal computer through a Riken Denshi TCDC-12-8000 transient recorder. Locally written software was employed for data collection and analysis. All the potential reported here are referred to an Ag/0.01 M $AgPF_6$, 0.1 M Bu_4NPF_6 (acetonitrile) reference electrode, against which the formal potential ($E^{O'}$) of the ferrocenium/ferrocene couple was +0.157 V in 0.1 M Bu_4NPF_6/acetonitrile.

Bulk controlled-potential electrolysis and coulometric experiments were carried out with a Nichia Keisoku NP-IR1000 potentiostat combined with a Fuso Electrochemical System HECS-343B digital coulometer. The working electrode was a reticulated vitreous carbon electrode (RVC 80-S) and the apparent volume was ca. 0.7 cm^3. The working compartment (5 cm^3) was separated from the counter compartment by a sintered-glass disk. After complete electrolysis (ca. 20 min), the working solution was transferred to a spectrometric cell through a stainless steel cannula and argon pressure. UV, visible, and near ir spectra of the electrolyzed solution were recorded on a Hitachi 330 spectrophotometer.

Other Measurements. ^1H NMR spectra were obtained at room temperature by using a JNM-EX400 FT-NMR spectrometer at 400 MHz with the sample solutions in CD_3CN. TMS was used as an internal standard. Electronic absorption spectra were recorded on a JASCO Ubest-30 spectrophotometer. Circular dichroism spectra were recorded on a JASCO J-500A spectropolarimeter.

^1H NMR line shape analysis to obtain rate constants for the ligand diamine ring interconversion was carried out using a computer program based on a modified Bloch equation for the two site exchange.[30] Rate constants were determined based on the optimal visual fits of the experimental and calculated spectra.

X-Ray Crystallography. X-Ray data of **1a**, **2**, and **3** were collected with graphite-monochromated Mo $K\alpha$ radiation on a Rigaku AFC-5R diffractometer at 20 °C. Each unit cell parameter was obtained by least-squares refinement of 25 reflections ($25 \leq 2\theta \leq 30°$). The intensities of three standard reflections for each compound, monitored every 150 reflections, showed no appreciable decay during the data collection. Absorption correction was made only for compound **3**.

The crystal structures were solved by standard heavy-atom procedures. The positional and thermal parameters were refined by the block-diagonal-matrix least-squares method. The minimized function was $\sum w(|F_o| - |F_c|)^2$, where $w^{-1} = \sigma^2(|F_o|) + (0.015|F_o|)^2$. No attempt was made to locate hydrogen atoms in the structure analysis. In the final cycle of the refinement, parameter shifts were less than 0.1σ. No correction was made for secondary extinction. The atomic scattering factors for neutral atoms, with correction for anomalous dispersion of Mo^0, W^0, and Cl^0, were used throughout the analysis.[31] Computational work was carried out by using standard programs in UNICS III[32] and ORTEP.[33] Further crystallographic data are given in Table 1. Listings of the non-hydrogen atom coordinates are given in Tables 2, 3, and 4. Anisotropic thermal parameters, full listings of bond distances and angles, and calculated and observed structure factors are deposited as Document No. 68005 at the Office of the Editor of Bull. Chem. Soc. Jpn.

Results and Discussion

Preparation. Oxomolybdenum(V) complexes that are stable in aqueous media, are almost exclusively those with a syn-di-μ-oxo core, *syn*-$Mo_2O_2(\mu\text{-}O)_2^{(2+)}$.

Table 1. Crystallographic Data for X-Ray Diffraction Studies

	1a	**2**	**3**
Formula	$C_{26}H_{34}Cl_5Mo_3N_6O_8$	$C_{27}H_{34}Cl_2Mo_2N_6O_{14}$	$C_{30}H_{34}Cl_2N_8O_{12}W_2$
FW	1023.68	929.38	1137.25
Cryst syst	Triclinic	Monoclinic	Triclinic
Space group	$P\bar{1}$	$P2/a$	$P\bar{1}$
a/Å	13.686(3)	17.862(2)	12.873(1)
b/Å	14.783(3)	9.422(2)	13.187(1)
c/Å	9.650(3)	11.285(2)	12.689(1)
α/deg	105.28(2)	90	97.80(1)
β/deg	101.85(2)	106.65(1)	116.08(1)
γ/deg	76.27(2)	90	83.96(1)
V/Å^3	1808.2(8)	1801.2(5)	1914.3(4)
Z	2	2	2
d_{calcd}/g cm^{-3}	1.880	1.714	1.973
Cryst. size/mm	0.33×0.73×0.33	0.27×0.40×0.27	0.23×0.23×0.38
Scan range/deg	1.0+0.4tan θ	1.0+0.5tan θ	1.2+0.4tan θ
Scan mode	ω–2θ	ω–2θ	ω–2θ
Scan speed/deg min^{-1}	6	8	6
$2\theta_{max}$/deg	60	60	60
μ(Mo $K\alpha$)/cm^{-1}	14.27	9.08	65.75
No. of unique rflns	11287	4611	11621
No. of obsd rflns	8640, $F_o>3\sigma(F_o)$	1896, $F_o>6\sigma(F_o)$	7308, $F_o>6\sigma(F_o)$
R[a)]	0.048	0.060	0.037
R_w[b)]	0.058	0.071	0.043

a) $R=\sum||F_o|-|F_c||/\sum|F_o|$. b) $R_w=[\sum w(|F_o|-|F_c|)^2/\sum w|F_o|^2]^{1/2}$.

If the preparation is carried out in aqueous media, the complexes with this core are usually obtained. In non-aqueous media, other structures such as monomeric and single-oxide-bridged dimeric oxomolybdenum complexes are often found. A hexadentate ligand, edta, gives a basket-type *syn*-$Mo_2O_2(\mu\text{-}O)_2^{(2+)}$ complex as prepared in aqueous medium. The ligand tpen and tppn which are structurally similar to edta and yet soluble in organic solvents, might give an opportunity to find other than the basket-type di-μ-oxo structure. Preparation of oxomolybdenum(V) complexes in aqueous media using monomeric oxomolybdenum(V) complex, $[MoCl_5O]^{2-}$, as a starting material, gave new tpen and tppn complexes with the $Mo_2O_2(\mu\text{-}O)_2^{(2+)}$ core. Attempts to use organic solvents for the preparation were unsuccessful in obtaining stable compounds of different structural types. The reaction of tpen and $(pyH)_2[MoCl_5O]$ in acetonitrile gave a purple side product, although the well-identified $Mo_2O_2(\mu\text{-}O)_2^{(2+)}$ complex was obtained eventually. Further study on this purple solid was difficult due to its instability even in organic solvents. It is concluded that the hexadentate ligands prefer to take the basket-type dinuclear structure with Mo–Mo single bond. For the preparation of oxotungsten(V) complexes, reaction of tpen or tppn with a mononuclear complex such as $[WCl_5O]^{2-}$ did not give any well-identified product in sufficiently high yield. Alternatively we used oxalate complex of $W_2O_2(\mu\text{-}O)_2^{(2+)}$[29] as a starting material; with this, use of organic solvents is not possible. The new oxotungsten(V) complexes were obtained by ligand substitution at the $W_2O_2(\mu\text{-}O)_2^{(2+)}$ core.

Description of the Structures. The structural analyses clearly show that all three complexes exhibit basket type dinuclear structures similar to those of oxomolybdenum(V) and oxotungsten(V) complexes with edta and pdta.[5—12] Structures of the tpen and tppn complexes of oxomolybdenum(V) and the tpen complex of oxotungsten(V) are given in Figs. 1, 2, and 3, respectively, with atomic numbering schemes.

In all the complexes, diamine part of the ligand take pseudo-gauche conformation. The complex cations with λ and δ pseudo-gauche conformations exist in equal amounts in each crystal of all three complexes. In the crystal of the Mo–tpen complex, cation of δ conformation is correlated with that with a λ conformation by a crystallographical inversion center. In the crystal of

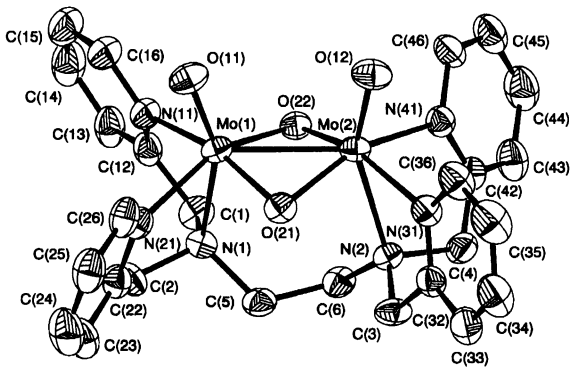

Fig. 1. Structure of the $[Mo_2O_2(\mu\text{-}O)_2(tpen)]^{2+}$ ion in **1a** and its atomic numbering scheme.

Table 2. Fractional Coordinates and Isotropic Thermal Parameters (Å^2) for $[Mo_2(O)_2(\mu\text{-}O)_2(\mu\text{-tpen})][MoCl_4O(H_2O)]Cl\cdot 2H_2O$ (**1a**)

Atom	x	y	z	B_{eq}
Mo(1)	0.10092(3)	0.82943(2)	0.25296(4)	2.44(1)
Mo(2)	0.24694(3)	0.88508(2)	0.44160(4)	2.30(1)
O(11)	0.0160(3)	0.9303(2)	0.2396(4)	3.9(1)
O(12)	0.2125(3)	1.0052(2)	0.4840(3)	3.6(1)
O(21)	0.1418(2)	0.8223(2)	0.4540(3)	2.8(1)
O(22)	0.2359(2)	0.8385(2)	0.2346(3)	2.6(1)
N(1)	0.1671(3)	0.6647(2)	0.1778(3)	2.5(1)
C(1)	0.2110(3)	0.6499(3)	0.0419(5)	3.2(1)
N(11)	0.0782(3)	0.7876(3)	0.0094(4)	3.1(1)
C(12)	0.1376(3)	0.7077(3)	−0.0578(5)	3.2(1)
C(13)	0.1348(4)	0.6807(4)	−0.2074(5)	3.9(1)
C(14)	0.0701(4)	0.7413(5)	−0.2907(6)	5.0(2)
C(15)	0.0092(4)	0.8234(4)	−0.2236(6)	5.0(2)
C(16)	0.0143(4)	0.8449(4)	−0.0733(5)	4.1(1)
C(2)	0.0804(3)	0.6123(3)	0.1378(5)	3.1(1)
N(21)	−0.0119(3)	0.7538(3)	0.2798(4)	2.8(1)
C(22)	0.0039(3)	0.6576(3)	0.2410(5)	3.0(1)
C(23)	−0.0499(4)	0.6053(4)	0.2866(6)	4.3(2)
C(24)	−0.1250(4)	0.6557(5)	0.3729(6)	5.1(2)
C(25)	−0.1413(4)	0.7555(4)	0.4130(6)	4.3(2)
C(26)	−0.0839(3)	0.8022(4)	0.3642(5)	3.5(1)
N(2)	0.3514(2)	0.7384(2)	0.4709(3)	2.4(1)
C(3)	0.3262(4)	0.7152(3)	0.5994(4)	3.1(1)
N(31)	0.2859(3)	0.8878(3)	0.6790(3)	2.8(1)
C(32)	0.3144(3)	0.8038(3)	0.7191(4)	2.9(1)
C(33)	0.3276(4)	0.7972(4)	0.8634(5)	4.1(1)
C(34)	0.3074(5)	0.8806(4)	0.9689(5)	4.9(2)
C(35)	0.2785(5)	0.9684(4)	0.9283(5)	4.9(2)
C(36)	0.2682(4)	0.9700(4)	0.7829(5)	3.9(1)
C(4)	0.4603(3)	0.7500(3)	0.5063(5)	3.2(1)
N(41)	0.4001(3)	0.8915(3)	0.4091(4)	2.7(1)
C(42)	0.4773(3)	0.8178(3)	0.4246(4)	2.9(1)
C(43)	0.5688(4)	0.8058(4)	0.3740(5)	4.0(1)
C(44)	0.5799(4)	0.8747(4)	0.3056(6)	4.8(2)
C(45)	0.5007(4)	0.9520(4)	0.2926(5)	4.6(2)
C(46)	0.4112(4)	0.9594(3)	0.3446(5)	3.5(1)
C(5)	0.2440(3)	0.6198(3)	0.2891(5)	2.9(1)
C(6)	0.3456(3)	0.6552(3)	0.3419(4)	2.8(1)
Mo(3)	0.25876(3)	0.27064(3)	0.10698(5)	3.45(1)
O(31)	0.1970(3)	0.2013(3)	−0.0288(4)	5.9(1)
O(32)	0.3461(3)	0.3690(3)	0.2889(4)	4.3(1)
Cl(1)	0.2658(1)	0.3828(1)	−0.0247(2)	6.0(1)
Cl(2)	0.1157(1)	0.3721(1)	0.2056(2)	5.9(1)
Cl(3)	0.2772(1)	0.1823(1)	0.2841(2)	5.49(4)
Cl(4)	0.4259(1)	0.1916(1)	0.0661(2)	5.83(5)
Cl(5)	0.3331(1)	0.4659(1)	0.6136(2)	6.1(1)
OW(1)	0.4844(3)	0.4464(3)	0.2154(5)	6.5(2)
OW(2)	0.4989(5)	0.6381(4)	0.0847(6)	8.8(2)

Table 3. Fractional Coordinates and Isotropic Thermal Parameters (Å^2) for $[Mo_2(O)_2(\mu\text{-}O)_2(\mu\text{-tppn})](ClO_4)_2\cdot 2H_2O$ (**2**)

Atom	x	y	z	B_{eq}
Mo	0.2259(1)	0.0740(1)	0.0958(1)	2.31(2)
O(11)	0.2200(5)	−0.1003(8)	0.1251(7)	3.8(3)
O(21)	0.1723(4)	0.1173(7)	−0.0739(7)	2.4(2)
N(1)	0.2069(5)	0.321(1)	0.1220(8)	2.5(3)
C(1)	0.2256(7)	0.350(1)	0.260(1)	3.1(4)
N(11)	0.2883(5)	0.116(1)	0.2905(8)	3.1(3)
C(12)	0.2889(6)	0.248(1)	0.335(1)	3.0(4)
C(13)	0.3406(8)	0.290(2)	0.450(1)	4.1(4)
C(14)	0.3911(8)	0.188(2)	0.521(1)	4.8(5)
C(15)	0.3882(8)	0.051(2)	0.477(1)	4.7(5)
C(16)	0.3373(7)	0.018(2)	0.361(1)	4.2(4)
C(2)	0.1207(6)	0.350(1)	0.067(1)	2.9(3)
N(21)	0.1096(5)	0.107(1)	0.1306(8)	2.7(3)
C(22)	0.0746(6)	0.237(1)	0.105(1)	2.7(3)
C(23)	−0.0030(6)	0.261(1)	0.111(1)	3.2(4)
C(24)	−0.0439(7)	0.148(1)	0.144(1)	3.6(4)
C(25)	−0.0073(7)	0.014(1)	0.174(1)	3.3(4)
C(26)	0.0705(7)	−0.002(1)	0.165(1)	3.2(4)
C(3)	0.2582(7)	0.423(1)	0.070(1)	3.1(4)
C(4)[a]	0.238(1)	0.583(3)	0.083(2)	4.1(8)
Cl(1)	0.0278(3)	−0.3846(4)	0.2892(3)	5.4(1)
O(31)	0.0444(9)	−0.356(1)	0.175(1)	9.5(5)
O(32)	0.0658(8)	−0.504(1)	0.345(1)	9.4(5)
O(33)	0.045(1)	−0.274(1)	0.374(1)	12.2(7)
O(34)	−0.0544(8)	−0.418(2)	0.252(1)	14.3(8)
OW	0.118(1)	−0.336(2)	0.637(1)	15.8(9)

a) Atomic occupancy is 0.5.

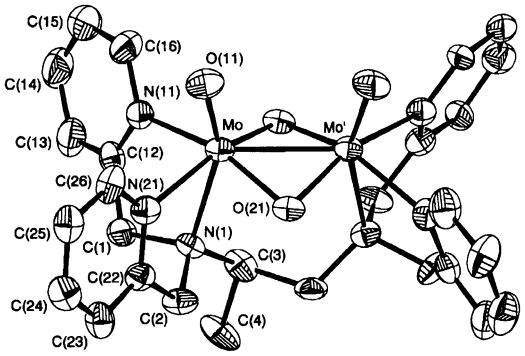

Fig. 2. Structure of the $[Mo_2O_2(\mu\text{-}O)_2(tppn)]^{2+}$ ion in **2** and its atomic numbering scheme.

the Mo–tppn complex where a crystal of the racemic tppn complex was used for the analysis, *R*-tppn and *S*-tppn complex cations respectively form columnar arrangements. Within the column, methyl substituents are disordered around the molecular two-fold axis in two carbon atoms of the diamine moiety with equal occupancy factors. A two-dimensional structure is formed from the columns of the complex cations of the same absolute configuration. The two dimensional sheets of the complexes of the *R*-tppn and the *S*-tppn appear alternately in the crystal. Figure 2 represents the *R*-tppn complex cation with methyl substituent at one of the carbon atoms of the diamine part, which takes λ-pseudo-gauche conformation.

Table 5 compares the selected bond-lengths and angles of the three complexes and the corresponding pdta complexes. Structural characteristics of the three new complexes are very similar to each other. A methyl substituent of tppn ligand thus does not give significant influence on the overall structure. Within the $M_2O_2(\mu$-

Table 4. Fractional Coordinates and Isotropic Thermal Parameters (Å^2) for $[W_2(O)_2(\mu\text{-}O)_2(\mu\text{-tpen})](ClO_4)_2\cdot 2CH_3CN$ (**3**)

Atom	x	y	z	B_{eq}
W(1)	0.26074(2)	0.25733(2)	0.36229(2)	2.99(1)
W(2)	0.30792(2)	0.17929(2)	0.19123(2)	2.98(1)
O(11)	0.3429(4)	0.1818(4)	0.4713(4)	4.6(2)
O(12)	0.3999(4)	0.0770(4)	0.2456(5)	4.6(2)
O(21)	0.1692(4)	0.1769(3)	0.2155(4)	3.3(1)
O(22)	0.3552(4)	0.3051(3)	0.2956(4)	3.3(1)
N(1)	0.1167(5)	0.3841(4)	0.2723(5)	3.3(2)
C(1)	0.1245(6)	0.4738(5)	0.3642(7)	4.1(2)
N(11)	0.3178(5)	0.3980(4)	0.4790(4)	3.5(2)
C(12)	0.2506(6)	0.4862(5)	0.4515(6)	4.1(2)
C(13)	0.2890(7)	0.5828(6)	0.5054(8)	5.4(3)
C(14)	0.4014(8)	0.5871(7)	0.5958(7)	5.7(3)
C(15)	0.4683(8)	0.4979(7)	0.6271(8)	5.9(3)
C(16)	0.4251(7)	0.4056(6)	0.5666(7)	4.8(2)
C(2)	0.0018(6)	0.3404(6)	0.2323(7)	4.3(2)
N(21)	0.1088(5)	0.2426(5)	0.3992(5)	4.5(2)
C(22)	0.0035(6)	0.2836(6)	0.3257(7)	4.8(3)
C(23)	−0.0969(8)	0.2687(7)	0.337(1)	7.3(4)
C(24)	−0.090(1)	0.2058(9)	0.421(1)	8.8(5)
C(25)	0.019(1)	0.1641(9)	0.498(1)	8.6(5)
C(26)	0.1199(9)	0.1848(7)	0.4866(8)	6.5(4)
N(2)	0.2111(5)	0.2983(4)	0.0534(4)	3.2(2)
C(3)	0.1709(7)	0.2421(5)	−0.0693(6)	4.0(2)
N(31)	0.2006(5)	0.0883(4)	0.0280(5)	3.6(2)
C(32)	0.1364(6)	0.1354(5)	−0.0694(6)	3.6(2)
C(33)	0.0476(7)	0.0891(6)	−0.1702(7)	4.8(3)
C(34)	0.0288(8)	−0.0125(7)	−0.1665(8)	5.7(3)
C(35)	0.0957(8)	−0.0618(6)	−0.0673(8)	5.6(3)
C(36)	0.1807(8)	−0.0096(5)	0.0300(7)	5.2(3)
C(4)	0.2988(7)	0.3715(5)	0.0655(6)	4.2(2)
N(41)	0.4283(5)	0.2224(4)	0.1230(5)	4.3(2)
C(42)	0.4081(7)	0.3112(6)	0.0761(6)	4.4(2)
C(43)	0.4841(9)	0.3490(8)	0.0420(8)	6.8(4)
C(44)	0.5891(9)	0.2881(9)	0.0603(9)	7.9(4)
C(45)	0.6084(9)	0.1955(9)	0.1073(9)	7.5(4)
C(46)	0.5270(7)	0.1635(7)	0.1400(8)	5.3(3)
C(5)	0.1245(7)	0.4279(5)	0.1729(6)	4.1(2)
C(6)	0.1082(6)	0.3560(5)	0.0601(6)	3.7(2)
Cl(1)	−0.2039(2)	0.5711(2)	0.2709(2)	5.7(1)
O(31)	−0.1319(7)	0.5743(7)	0.2134(7)	11.1(4)
O(32)	−0.276(1)	0.4956(8)	0.205(1)	16.2(6)
O(33)	−0.1386(8)	0.5427(8)	0.3829(7)	12.6(4)
O(34)	−0.265(1)	0.6620(7)	0.270(1)	15.3(6)
Cl(2)	−0.2254(2)	0.3111(2)	−0.1526(2)	6.3(1)
O(41)	−0.178(1)	0.3832(9)	−0.0559(9)	14.1(5)
O(42)	−0.148(1)	0.308(1)	−0.203(1)	18.6(8)
O(43)	−0.240(2)	0.2248(8)	−0.134(2)	28(1)
O(44)	−0.319(1)	0.356(1)	−0.225(1)	20.2(7)
C(51)	0.456(1)	0.1582(9)	−0.237(1)	9.0(5)
C(52)	0.386(1)	0.1088(9)	−0.203(1)	9.8(5)
N(53)	0.330(1)	0.070(1)	−0.175(1)	16.3(8)
C(61)	0.379(1)	0.906(1)	0.434(1)	11.4(7)
C(62)	0.292(2)	0.908(1)	0.460(2)	17(1)
N(63)	0.196(2)	0.931(1)	0.458(2)	19(1)

$O)_2^{(2+)}$ cores, metal-ligand bond lengths are slightly longer for the tungsten complex, while the bond-angles are virtually the same. Consequently, metal-to-metal

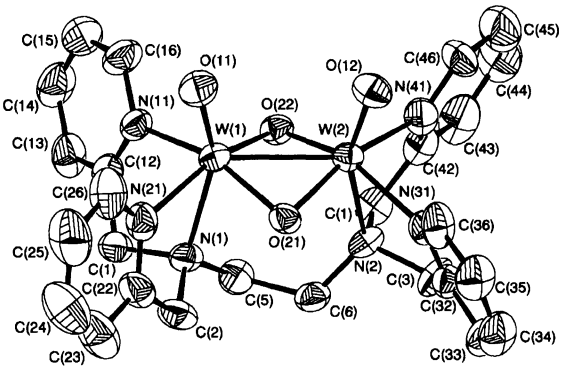

Fig. 3. Structure of the $[W_2O_2(\mu\text{-}O)_2(tpen)]^{2+}$ ion in **3** and its atomic numbering scheme.

distance is ca. 0.02 Å longer for the tungsten complex. The metal-metal distances of the Mo–tpen, Mo–tppn, and W–tpen complexes are 2.546(1), 2.541(2), and 2.561(1) Å respectively, indicating formal metal–metal single bonds as suggested for other $M_2O_2(\mu\text{-}O)_2^{(2+)}$ complexes. Metal-ligand bond distances involving the chelating ligands are almost identical among the three complexes.

Structural characteristics of the three complex cations are also similar to the corresponding molybdenum(V) and tungsten(V) complexes of edta and pdta.[7,8,11] The metal–metal distances are slightly longer (ca. 0.01 Å) for the complexes of the tpen series. A notable difference is seen in the bond-lengths of the metal–N(amine) and metal–basal ligand atoms (trans to the bridging oxides) as well as the N(pyridyl)–M–N(pyridyl) angles. This may be explained by considering the weaker basicity of the donor groups and the repulsion of bulky pyridyl groups of tpen and tppn ligands. Significant difference in the structures of the two series of complexes is found in the asymmetric distortion. Figure 4 shows the view along the metal–metal axis of the Mo–tpen, –*R*-tppn and –*R*-pdta complexes. For the Mo–*R*-tppn complex, two Mo–N(amine) bonds are clearly twisted and each pair of the other three bonds including Mo–O(oxo) are also twisted slightly to the same direction as the Mo–N(amine) pair. The distortion should be closely related to the fixed pseudo-gauche conformation of the diamine moiety. It is seen that the two octahedrons are twisted clockwise (this configuration has been defined as *Λ* in the previous paper[11])

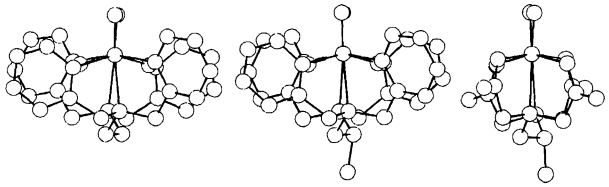

Fig. 4. The projections along Mo–Mo axes of $[Mo_2O_2(\mu\text{-}O)_2(tpen)]^{2+}$ (left), $[Mo_2O_2(\mu\text{-}O)_2(R\text{-tppn})]^{2+}$ (middle) and $[Mo_2O_2(\mu\text{-}O)_2(R\text{-pdta})]^{2-}$ (right).

Table 5. Comparison of Selected Bond Lengths and Angles of $[M_2(O)_2(\mu\text{-}O)_2(tpen)]^{2+}$, $[M_2(O)_2(\mu\text{-}O)_2(tppn)]^{2+}$ and $[M_2(O)_2(\mu\text{-}O)_2(pdta)]^{2-}$ (M=Mo,W)[a,b]

	Complex				
	Mo–tpen	Mo–tppn	W–tpen	Mo–pdta[c]	W–pdta[d]
	Bond lengths (Å)				
M–M	2.546(1)	2.541(2)	2.561(1)	2.533(2)	2.5472(6)
M–O_t	1.681[5]	1.684(8)	1.701[5]	1.68(2)	1.69[1]
M–O_b	1.926[4]	1.925[4]	1.946[2]	1.93[1]	1.96[4]
M–N	2.354[7]	2.386(9)	2.349[5]	2.47[2]	2.43[2]
M–L_a	2.205[5]	2.194(9)	2.186[5]	2.11(2)	2.10[1]
M–L_b	2.239[5]	2.223(9)	2.232[2]	2.11[2]	2.09[6]
	Bond angles (deg)				
M′–M–O_t	104.5[2]	102.8(3)	103.4[5]	100[2]	99.9[4]
M′–M–O_b	48.6[2]	48.7[1]	48.9[1]	48.9[1]	50[1]
M′–M–N	101.5[2]	101.5(2)	101.3[2]	100.7[6]	101[2]
M′–M–L_a	128.2[6]	131.1(3)	129.6[3]	139.7[1]	136[1]
M′–M–L_b	132.0[9]	134.7(2)	132.0[5]	136[1]	135[1]
O_t–M–O_b	112.5[2]	111.2(3)	112.3[4]	106.6[2]	110[2]
O_t–M–O'_b	110.3[1]	110.1(4)	110.5[2]	111[2]	112[2]
O_t–M–N	153.8[1]	155.5(4)	155.0[3]	159[2]	159[2]
O_t–M–L_a	93[1]	91.2(4)	92.7[1]	89.5[6]	90.3[6]
O_t–M–L_b	88.4[5]	89.4(4)	89.1[5]	92[3]	93[2]
O_b–M–O'_b	92.4[2]	92.2(3)	92.3[5]	93.0[2]	92[1]
O_b–M–N	82.1[4]	82.5(3)	81.2[3]	87.5[1]	85.2[8]
O'_b–M–N	89.9[7]	88.8(3)	89.2[1]	83.5[8]	82[1]
N–M–L_a	73.8[2]	75.4(3)	74.8(2)	74.4(6)	73.8[3]
N–M–L_b	71.2[4]	70.8(3)	71.0[2]	72.7[2]	72.2[7]
L_a–M–L_b	96.3[4]	92.2(3)	95.1[4]	82.1[8]	86.1[4]
	Torsion angles (deg)[e]				
O_t–M–M′–O'_t	2.8(2)	1.5(4)	2.3(3)	−5.4(8)	−2.7(5)
L_a–M–M′–L'_b	7.3(2)	2.6(6)	6.0(3)	−6.8(11)	−4.0(6)
L_b–M–M′–L'_a	8.2(2)	2.6(6)	6.4(3)	−8.6(10)	−10.4(7)
N–M–M′–N′	11.1(1)	8.8(3)	11.3(2)	−5.4(6)	−4.8(3)
L_a–L_b–L'_a–L'_b	8.4(1)	3.1(4)	6.4(2)	−8.6(7)	−7.1(4)
L_a–Cl_a–$C2_a$–N	−38[1]	−34.26[4]	−36.2[2]	29[5]	27[7]
L_b–Cl_b–$C2_b$–N	−27.6[9]	−27.49[3]	−27.89[2]	−28[1]	−24[3]

a) Numbers in square brackets are root-mean-square derivations of the individual values (either 2 or 4 in number) from their mean. b) Atomic labeling: O_t and O_b represent terminal and bridging oxides, respectively. L's are basal coordinating atoms (N for tpen and tppn, and O for pdta complexes). N is diamine nitrogen. The atoms C1 and C2 are 2-pyridyl or carboxyl carbons, and pyridylmethyl or carboxymethyl carbons, respectively. Two halves of the complex ions are distinguished by prime. Two different pyridylmethyl or carboxymethyl arms of the half unit are distinguished by a and b. c) Refs. 8 and 25. d) Ref. 11. e) Plus sign for the clockwise torsion angle (Λ configuration).

along the Mo–Mo axis when the pseudo-gauche conformation is λ. The distortion observed for the Mo–tppn complex is not due to crystal packing, because such distortion is also observed for the two tpen complexes in a similar manner (Fig. 4). For the enantiomer with λ conformation of the tpen diamine moiety, the twist along both the Mo–Mo and W–W axes is clockwise (Λ configuration). These observations are in sharp contrast to the steric structures of $[M_2O_2(\mu\text{-}O)_2(R\text{-pdta})]^{2-}$ (M=Mo, W), where all the four pairs of the bonds are twisted anti-clockwise. (Δ configuration)[8,11] It is difficult to state unambiguously the reason for the different asymmetric distortion between the pdta and the tppn complexes of the same *R*-absolute configuration of the ligands. Close examination of bond lengths and angles of the five membered chelate rings, N–CH_2–C_5H_4N in the tppn and N–CH_2–COO^- in the pdta complexes indicates very similar structural parameters. The torsion angles within the pseudo-gauche structures of the two series of the complexes do not show any significant difference. Table 5 indicates, however, several structural characteristics which are closely related to the asymmetric distortion. Three points have been mentioned above; namely, the N(pyridyl)–Mo–N(pyridyl) angles are significantly larger for the tppn complex, the basal bond lengths of the tppn complex are consider-

ably longer than those of the pdta complex, and Mo–N-(amine) bond lengths are shorter for the tppn complex. In addition to these points, one significant feature is noted. As Fig. 5 shows the two five membered chelate rings, Mo–N–CH_2–C_6H_4N–Mo, at one Mo atom, are skewed to the same direction; namely one chelate ring is oriented to the outside of the N–Mo–N moiety, while the other is oriented to the inside. On the contrary, both the five chelate membered rings, Mo–N–CH_2COO–Mo, skewed to the outside of the O–Mo–O moiety. These structural features as well as the fixed pseudo-gauche ring of the diamine part would be responsible for the observed different asymmetric distortion of the two complexes. Circular dichroism spectra indicate that the distortion is retained in solution (vide infra).

$[Mo_2O_2(\mu\text{-}O)_2(tpen)]^{2+}$ crystallized as a salt of $[MoCl_4O(H_2O)]^-$. Structure of the complex anion is almost identical with the structure of the same anion in a salt, $[As(C_6H_5)_4][MoCl_4O(H_2O)]$.[34]

^{1}H NMR Spectra. The ^{1}H NMR signals of the four new complexes in acetonitrile appear in the region expected for a diamagnetic complex, indicating that they have no unpaired electrons. This is consistent with the formal metal–metal single bond. Spectra of the two tpen complexes show temperature dependence (Fig. 6), while those of the tppn complexes do not in the temperature range from 60 to −40 °C. Table 6 summarizes the chemical shifts of the complexes. For the tpen complexes, those at 60 and −40 °C are given.

It was reported that the ^{1}H and ^{13}C NMR spectra of $[M_2O_2(\mu\text{-}O)_2(edta)]^{2-}$ (M=Mo, W) show temperature dependence and those of the pdta analogs do not.[11,26] The temperature dependence was interpreted in terms of the pseudo-gauche conformational inversion of the

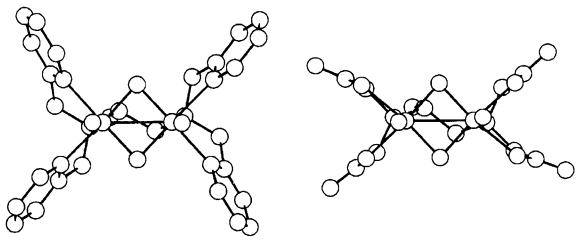

Fig. 5. The projections on the mean planes of four basal atoms for $[Mo_2O_2(\mu\text{-}O)_2(R\text{-tppn})]^{2+}$ (left) and $[Mo_2O_2(\mu\text{-}O)_2(R\text{-pdta})]^{2+}$ (right).

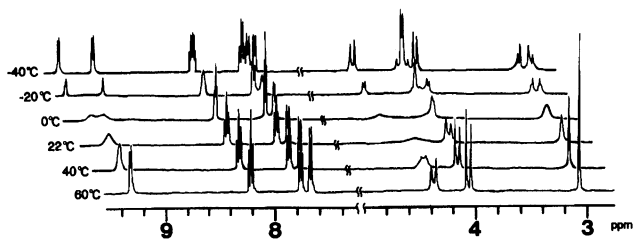

Fig. 6. ^{1}H NMR spectra of $[Mo_2O_2(\mu\text{-}O)_2(tpen)]^{2+}$ in CD_3CN at various temperatures.

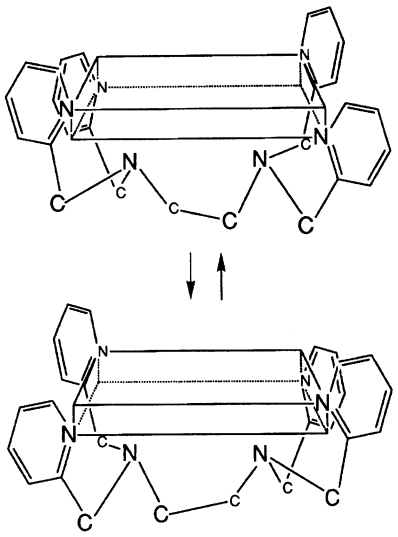

Fig. 7. Schematic view of the conformational inversion of $[M_2O_2(\mu\text{-}O)_2(tpen)]^{2+}$ (M=Mo,W) (core structure, $M_2O_2(\mu\text{-}O)_2$ is omitted for clarity).

diamine part of edta ligand. The inversion is not possible for the pdta complexes, because the methyl substituent prefers to take a fixed pseudo-gauche conformation and would cause steric hindrance against the inversion. Temperature dependence of the ^{1}H NMR spectra of tpen complexes is interpreted similarly on the basis of the pseudo-gauche conformational inversion which is illustrated in Fig. 7. Figure 6 shows that all the signals observed at 60 °C cause broadening as temperature decreases and split into two groups each at lower temperatures. The pseudo-gauche conformational inversion is rapid with respect to ^{1}H NMR time scale at 60 °C. Four protons of the diamine part and four pyridylmethyl groups are respectively equivalent. At −40 °C, the inversion is frozen and each of them is now located in two chemically non-equivalent sets of circumstances. The AB pattern of pyridylmethyl methylene groups at ca. 4.4 ppm at 60 °C is not symmetrical in shape. This may be due to long-range coupling of the doublet at lower magnetic field with pyridyl 6-H signal at 9.3 ppm. At the lowest temperature, two AB patterns are observed, one of which is composed of two protons with very close chemical shifts. The ethylene singlet signal at ca. 3.0 ppm at 60 °C becomes AB pattern at lower temperatures.

Rates of the inversion at 40, 22, 0, and −20 °C were obtained from the shape of pyridyl 6-H signals by a computer program based on the modified Bloch equation for the two site exchange.[30] From the temperature dependence of the exchange rate constants, activation parameters $\Delta H^\ddagger$ and $\Delta S^\ddagger$ were evaluated. Rate constants and activation parameters are summarized in Table 7, together with the corresponding values of the edta complexes. The most remarkable difference between the two ligand systems are seen in activation parameters. The tpen complexes give significantly large $\Delta H^\ddagger$ and more

Table 6. ^{1}H NMR Chemical Shifts (δ/ppm) of $[M_2O_2(\mu\text{-}O)_2(tpen)]^{2+}$ and $[M_2O_2(\mu\text{-}O)_2(tppn)]^{2+}$ (M=Mo,W) in CD_3CN

		Complex					
		Mo–tpen		W–tpen		Mo–tppn	W–tppn
		T/K	T/K	T/K	T/K	T/K	T/K
Assignment		233	333	233	333	298	298
Pyridyl 6-H	(4H)	9.45(d) 9.14(d)	9.33(d)	9.50(d) 9.11(d)	9.33(d)	9.44(m) 9.15(m)	9.50(m) 9.12(m)
Pyridyl 4-H	(4H)	8.25(t) 8.21(t)	8.22(t)	8.26(t) 8.22(t)	8.21(t)	8.26—8.16(m)	8.27—8.19(m)
Pyridyl 5-H	(4H)	7.79(t) 7.77(t)	7.78(t)	7.78(t) 7.77(t)	7.75(t)	7.78—7.74(m)	7.74—7.62(m)
Pyridyl 3-H	(4H)	7.72(d) 7.66(d)	7.68(d)	7.75(d) 7.65(d)	7.68(d)	7.66(m)	7.46(m)
Pyridylmethyl	(4H)	4.57(d) 4.00(d)	4.38(d)	4.64(d) 4.12(d)	4.41(d)	4.57—3.88(m)	4.69—3.97(m)
	(4H)	4.15(d) 4.09(d)	4.07(d)	4.21(d) 4.16(d)	4.15(d)		
Ethylene	(4H)	3.11(d) 2.95(d)	3.08(s)	3.09(d) 2.84(d)	2.99(s)		
Methylene	(2H)					3.33—3.20(m)	3.34—3.22(m)
Methine	(1H)					2.63(d)	2.74(d)
Methyl	(3H)					1.27(d)	1.31(d)

Table 7. Rate Constants and Activation Parameters for the Asymmetric Inversion for $[M_2(O)_2(\mu\text{-}O)_2(tpen)]^{2+}$ and $[M_2(O)_2(\mu\text{-}O)_2(edta)]^{2-}$ (M=Mo,W)

Complex	T/K	k/s^{-1}	$\Delta H^{\ddagger}$/kJ mol^{-1}	$\Delta S^{\ddagger}$/J K^{-1} mol^{-1}
Mo–tpen	253	6.25	86.6±4.7	+113.5±2.7
	273	1.39×10^2		
	295	1.67×10^3		
	313	2.50×10^4		
W–tpen	253	8.33	80.9±5.2	+93.9±3.0
	273	1.85×10^2		
	295	1.56×10^3		
	313	2.08×10^4		
Mo–edta[a,b]	298	5.10×10^2	54±8	+12.3±0.2
W–edta[a,b]	298	2.87×10^2	36±2	−53±5

a) Ref. 11. b) In D_2O.

positive $\Delta S^{\ddagger}$ values than those of the edta complexes. Thus, while the inversion rate constants of the tpen and the edta complexes are within an order of magnitude at room temperature, they should be significantly different at higher temperatures. For the edta complexes, intramolecular conformational change without bond break was suggested.[11,26] Large positive $\Delta S^{\ddagger}$ and large $\Delta H^{\ddagger}$ values for the tpen complexes are not consistent with such a mechanism, rather they are reminiscent of a dissociative ligand substitution reaction.[35,36] We conclude that the inversion of the tpen complexes proceeds through dissociative bond-break of a basal bond. Since acetonitrile is not expected to be a significantly better nucleophile than water to assist the formation of a transition state with partially broken basal bond, the different solvent media applied in the two different series of the complexes are not responsible for the different kinetic parameters. The longer equatorial bond-lengths of the tpen complexes may facilitate more easy bond-breaks than the edta complexes. The different asymmetric distortion found for the tpen complexes (vide supra) appears to indicate a more difficult intramolecular inversion without bond-break. The kinetic parameters between the two tpen complexes are not significantly different. This is reasonable in view of very similar steric structures of the Mo and W tpen complexes.

Electrochemistry. Cyclic voltammograms (CV) of the two tpen complexes were measured in acetonitrile at 25 °C. Figure 8a shows a cyclic voltammogram of $[Mo_2O_2(\mu\text{-}O)_2(tpen)]^{2+}$ at a conventionaly-sized glassy carbon electrode. A negative potential scan initiated at −0.8 V and the following positive scan reversed at −2.2 V with a scan rate of 50 mV s^{-1} revealed two chemically reversible redox couples with formal potentials of

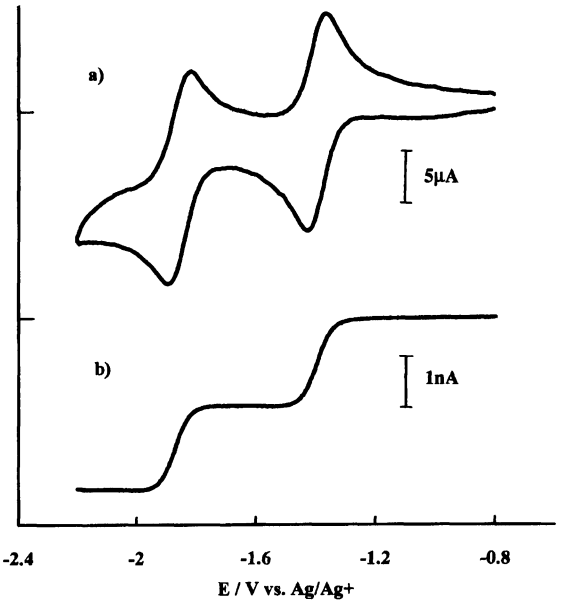

Fig. 8. Cyclic (a) and steady state (b) voltammograms of 0.82 mM $[Mo_2O_2(\mu\text{-}O)_2(tpen)]^{2+}$ in acetonitrile/0.1 M Bu_4NPF_6 with a scan rate of 50 mV s^{-1}.

−1.40 and −1.86 V, respectively. The peak-to-peak separations of 62 and 75 mV indicate the electrochemically reversible and quasi-reversible one-electron processes for the first and second redox couples, respectively. Bulk controlled potential coulometry with a reticulated vitreous carbon at an applied potential of −1.65 V confirmed the first reduction to be a one-electron process (n=1.00).

Figure 8b illustrates a steady state voltammogram of $[Mo_2O_2(\mu\text{-}O)_2(tpen)]^{2+}$ at a carbon microdisk electrode in the same solution. There were two consecutive reduction waves with half-wave potentials of −1.39 and −1.86 V, respectively, which are compatible with the corresponding formal potentials obtained in cyclic voltammetry. The steady state plateau for the first and second reduction waves are virtually identical, as would be anticipated. These voltammetric and coulometric results establish the stepwise one-electron reductions through a Mo_2(IV,V) intermediate to a Mo_2(IV,IV) species.

The two redox couples are very well separated ($\Delta E^{O'}$=0.46 V) and the comproportionation constant (K_{com}) represented by the following equations is calculated to be 6.2×10^7.

$$Mo_2(V,V) + Mo_2(IV,IV) = 2Mo_2(IV,V) \quad (1)$$

$$K_{com} = \exp(F\Delta E^{O'}/RT) \quad (2)$$

Considering the thermodynamically large stability of the mixed-valence complex, Mo_2(IV,V), it should be feasible to study the nature of the interaction of the unpaired electron with the two molybdenum centers by electronic spectroscopy. The controlled potential electrolysis at −1.65 V, during which the solution color changed from yellow to brownish green, yielded the mixed valence Mo_2(IV,V) species, which is stable in an inert atmosphere but is readily reoxidized to Mo_2(V, V) with a partial decomposition when exposed to air. The electronic absorption spectrum of the mixed valence species will be discussed in a later section.

In contrast to the reversible reduction of the Mo–tpen complex, the W–tpen complex showed irreversible reduction processes. The W–tpen complex exhibits a reduction wave (E_{pc}) at −1.68 V, but no corresponding reoxidation wave was observed. The second reduction wave was observed at ca. −1.89 V, but was poorly resolved. Reduction products of the W complexes appear to be unstable electrochemically.

The oxidation process was observed as irreversible for both the Mo and W complexes. Oxidation potential of the W complex (+1.2 V) appears at less positive potentials than the Mo complex (+1.6 V). It is clear that the Mo complex is more easily reduced and more difficult to be oxidized, as compared with the corresponding W complex. This is a general trend observed for analogous compounds of second and third transition metals of the same family.

The edta complex $[Mo_2O_2(\mu\text{-}O)_2(edta)]^{2-}$ reversibly reduced at −2.22 V vs. SCE in acetonitrile; this was a one-electron process as confirmed by comparison of its peak current parameters with that for the oxidation of ferrocene.[37] No second reduction wave was observed. The first redox potential may be compared with the corresponding potential of $[Mo_2O_2(\mu\text{-}O)_2(tpen)]^{2+}$ at −1.89 V vs. SCE, which was estimated by converting the value vs. Ag/Ag^+ by using $E^{O'}$ value of Fc/Fc^+ as a reference. It is clear that the tpen complex is more easily reduced than the edta complex.

Since it was reported that $[Mo_2O_2(\mu\text{-}O)_2(edta)]^{2-}$ is reduced to Mo_2(III,III) by a one-step four-electron process coupled with protonation at terminal oxides in aqueous media,[38—40] we have tried to see the influence of added acid on the redox behavior of the tpen complex in acetonitrile. In the case of the oxo-bridged dinuclear ruthenium(III) complexes, $[Ru_2(\mu\text{-}O)(\mu\text{-}CH_3COO)_2(2,2'\text{-bipyridine})_2(L)_2]^{2+}$ (L = pyridine, imidazole, 1-methylimidazole, etc.) in acetonitrile, protonation at the oxide bridge is coupled with the reduction to cause significant positive shift of the reduction potentials of Ru_2(III,III)/(II,III) and Ru_2(II,III)/(II,II) couples with increasing reversibility.[41] Addition of p-toluenesulfonic acid to the acetonitrile solution of $[Mo_2O_2(\mu\text{-}O)_2(tpen)]^{2+}$ did not cause any simple shift in reduction potentials. Rather, a complicated reduction pattern was observed, suggesting acid-catalyzed decomposition of reduction products.

Electronic Absorption Spectra. Electronic absorption spectra of the two tppn complexes in acetonitrile are shown in Fig. 9, together with their circular dichroism (CD) spectra. The absorption spectra of the tpen complexes of oxomolybdenum(V) and oxotungsten(V) are similar to those of the respective tppn

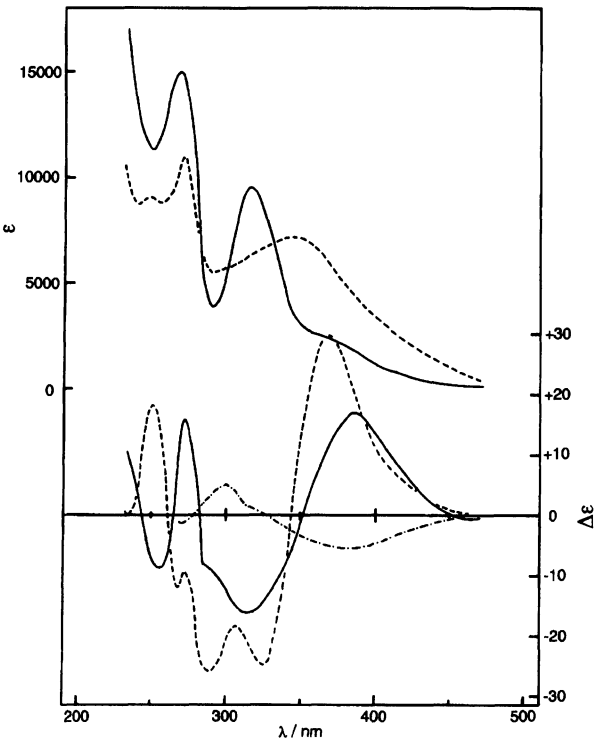

Fig. 9. Electronic (upper) and circular dichroism (lower) spectra of $[Mo_2O_2(\mu\text{-}O)_2(R\text{-tppn})]^{2+}$ (—) and $[W_2O_2(\mu\text{-}O)_2(R\text{-tppn})]^{2+}$ (---) in acetonitrile, and circular dichroism spectrum of $[Mo_2O_2(\mu\text{-}O)_2(R\text{-pdta})]^{2-}$ in water (–·–).

complexes. The spectra are compared with those of the edta or pdta complexes, $[M_2O_2(\mu\text{-}O)_2(\text{edta or pdta})]^{2-}$ (M=Mo, W) in water. We found that both absorption and CD spectra of $[W_2O_2(\mu\text{-}O)_2(R\text{-tppn})]^{2+}$ do not show significant solvent dependence in acetonitrile and water, and the different solvent media used for the measurements of the two series of the complexes are not important in interpreting the spectra.

In the previous studies of the absorption and CD spectra of the $Mo_2O_2(\mu\text{-}O)_2^{(2+)}$ complexes of optically active ligands,[25] it was concluded that the absorption bands of the $Mo_2O_2(\mu\text{-}O)_2^{(2+)}$ complexes can be classified into several groups regardless of the type of non-oxo ligands. These groups of absorption bands are assigned to transitions essentially within the core $Mo_2O_2(\mu\text{-}O)_2^{(2+)}$, i.e. transitions from occupied Mo–Mo σ-bonding orbital to upper bonding and *anti*-bonding Mo–Mo π-orbitals and σ-*anti*-bonding orbital, on the basis of the molecular orbital consideration reported earlier.[42,43] The spectra of $[W_2O_2(\mu\text{-}O)_2(\text{edta})]^{2-}$ and its *R*-pdta analog were also interpreted similarly by taking into account the blue shift of each band of the $Mo_2O_2(\mu\text{-}O)_2^{(2+)}$ counterparts.[11]

Electronic absorption bands of the tpen and tppn complexes of $Mo_2O_2(\mu\text{-}O)_2^{(2+)}$ and $W_2O_2(\mu\text{-}O)_2^{(2+)}$ are classified into three groups; these are summarized in Table 8. The classification was made by comparing peak positions and intensities with those of the corresponding edta complexes. It should be noted that CD signs of each band of the *R*-tppn complex are opposite to those of the corresponding band at similar transition energy and intensity (Fig. 9). It was pointed out earlier that CD signs of the optically active $Mo_2O_2(\mu\text{-}O)_2^{(2+)}$ complexes are related to asymmetric distortion around the metal–metal axis.[25] Since the asymmetric distortion of the two complexes are in opposite directions, it is reasonable that the corresponding bands of *R*-pdta and *R*-tppn show CD signs opposite to each other.

The spectral pattern of $[W_2O_2(\mu\text{-}O)_2(\text{tpen or } R\text{-tppn})]^{2+}$ complex is apparently different from that of $[Mo_2O_2(\mu\text{-}O)_2(\text{tpen or } R\text{-tppn})]^{2+}$. The former exhibits one broad band which apparently corresponds to a higher energy sharp band of the $Mo_2O_2(\mu\text{-}O)_2^{(2+)}$ complex. With the aid of the CD spectra, however, we concluded that the band at 385 nm (shoulder) (positive CD sign) and 315 nm (negative CD sign) of the Mo complex shift to shorter and longer wavelengths, respectively, in the W complex. Thus the apparently very broad band at 343 nm of the W complex is a composite of the two transitions.

Electronic spectra of the mixed valence $Mo_2(IV,V)$ complex is given in Fig. 10, which was obtained by the use of spectroelectrochemical techniques. The reduced complex exhibits three distinctive bands at 373 nm (ε= 5020 $mol^{-1}\,cm^{-1}\,dm^3$), 794 nm (4120), and 1400 nm (630) with prominent shoulder at 480 nm (2700). The absorption spectrum of $[Mo_2^{IV,V}O_2(\mu\text{-}O)_2(\text{edta})]^{3-}$ was obtained by the use of pulse radiolysis of aqueous solution of $[Mo_2^{V}O_2(\mu\text{-}O)_2(\text{edta})]^{2-}$.[44] The spectrum with several bands in the range from 400 to 600 nm with ε of less than 600 $mol^{-1}\,cm^{-1}\,dm^3$ and no band in longer wave-length region, is significantly different from that of $[Mo_2^{IV,V}O_2(\mu\text{-}O)_2(\text{tpen})]^{+}$ and we were unable to make meaningful comparisons.

According to the molecular orbital calculation of

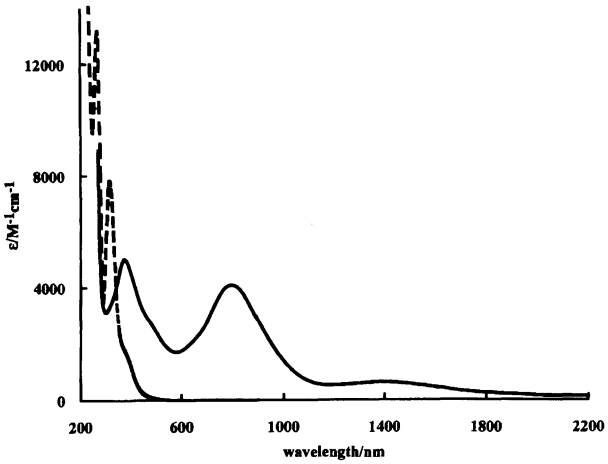

Fig. 10. Electronic spectra of $[Mo_2O_2(\mu\text{-}O)_2(\text{tpen})]^{2+}$ (---) and the one-electron reduction product (—) in acetonitrile/0.1 M Bu_4NPF_6.

Table 8. Electronic Absorption and CD Spectral Data for $[M_2(O)_2(\mu\text{-}O)_2(R\text{-tppn})]^{2+}$ and $[M_2(O)_2(\mu\text{-}O)_2(R\text{-pdta})]^{2-}$ and Electronic Absorption Spectral Data for $[M_2(O)_2(\mu\text{-}O)_2(\text{tpen})]^{2+}$ (M=Mo,W)[a]

Complex	Ligand	I		II	III
	Electronic absorption data: λ_{max}/nm (ε/M^{-1} cm^{-1})				
Mo–tpen	267(16000)	315(9500)		380s(1900)	
Mo–tppn	268(15000)	315(8800)		385s(1500)	
Mo–pdta[b,d]		298(10000)		388(398)	481s(100)
W–tpen	271(11000)		346(7900)		
W–tppn	271(10000)		343(7200)		
W–pdta[c,d]		277(12000)		342(1000)	420s(347)
	CD data: λ_{max}/nm ($\Delta\varepsilon$/M^{-1} cm^{-1})				
Mo–tppn		315(−16.3)		385(+17.0)	
Mo–pdta[b,d]		300(+5.1)		385(−5.5)	481s(−0.48)
W–tppn		325(−24.7)		367(+29.7)	
W–pdta[c,d]		292(+0.57)		357(−2.93)	444s(−0.61)

a) s indicates shoulder. b) Ref. 25. c) Ref. 11. d) In H_2O.

$[Mo_2O_2(\mu\text{-}O)_2(S\text{-cysteinato})_2]^{2-}$, LUMO is a π-bonding orbital with several orbitals with π- and σ-character within narrow energy range.[42] From the excellent reversible behavior of one-electron reduction of $[Mo_2^{V}O_2(\mu\text{-}O)_2(\text{tpen})]^{2+}$, the basic structure should be maintained in the reduced species which is thus formulated as $[Mo_2^{IV,V}O_2(\mu\text{-}O)_2(\text{tpen})]^{+}$. If the molecular orbital treatment is applicable to the present tpen complex, the unpaired electron would occupy a π-bonding orbital. Thus the Mo_2(IV,V) complex could have Mo–Mo bond of 1.5 order. As far as the molecular orbital scheme holds, absorption bands may correspond to the transitions from the occupied π-bonding orbital to upper π-bonding and antibonding orbitals.

Alternatively, a broad absorption centered at 1400 nm (ε=630 mol^{-1} dm^3 cm^{-1}) of the mixed-valence complex may be treated within the theories for an inter-valence band. Namely, it is assumed that the band at 1400 nm is attributed to the intervalence electron transfer transition between the mixed valence molybdenum centers. A gaussian function analysis for this band gave the half-width ($\Delta\nu_{1/2}$=2540 cm^{-1}) and the molar absorption coefficient (ε=578 mol^{-1} dm^3 cm^{-1}) at this maximum (ν_{max}=7040 cm^{-1}). The $\Delta\nu_{1/2}$ value is substantially smaller than the calculated value of 3780 cm^{-1} using the Hush relation[45] for class II compounds according to the Robin and Day classification,[46] suggesting a delocalized system close to class III. These results as well as the large comproportionation constant for the mixed-valence species are clear evidence for the electron-delocalization and metal–metal coupling between the two molybdenum centers. It is thus reasonable to assume that the molecular orbital approximation mentioned above, which is based on metal–metal bonding interaction, is valid for the present mixed-valence system.

This work was supported by a Grant-in-Aid for Scientific Research No. 05225201 on Priority Area of "New Development of Organic Electrochemistry" and a Grand-in-Aid for Scientific Research No. 05403008 from the Ministry of Education, Science and Culture. A research grant from Mitsubishi Foundation is also gratefully acknowledged. The authors are grateful to Dr. Masaaki Abe of Institute for Molecular Science for his assistance and helpful discussions on the ^{1}H NMR line shape analysis. They are also grateful to Processor F. Morita of the Department of Chemistry, Hokkaido University for the measurement of circular dichroism spectra.

References

1) E.I. Stiefel, *Prog. Inorg. Chem.*, **22**, 1 (1977).
2) Z. Dori, *Prog. Inorg. Chem.*, **28**, 239 (1981).
3) Some recent examples: a) V. S. Joshi, M. Nandi, H. Zhang, B. S. Haggerty, and A. Sarkar, *Inorg. Chem.*, **32**, 1301 (1993); b) F. A. Cotton, R. L. Luck, and C. S. Miertschin, *Inorg. Chem.*, **30**, 1155 (1991); c) B. Kamenar, B. Kaitner, and N. Strukan, *Croat. Chim. Acta*, **64**, 329 (1991); d) D. Coucouvanis, A. Toupadakis, J. D. Lane, S. M. Koo, C. G. Kim, and A. Hadjikyriacou, *J. Am. Chem. Soc.*, **113**, 5271 (1991); e) C. G. Kim and D. Coucouvanis, *Inorg. Chem.*, **32**, 2232 (1993); f) S. Stotzel, K. Wieghardt, and B. Nuber, *Inorg. Chem.*, **32**, 2128 (1993); g) S. G. Jonasdottir, C. G. Kim, and D. Coucouvanis, *Inorg. Chem.*, **32**, 3591 (1993); h) C. Simonnet-Jegat, R. A. Toscano, F. Robert, J.-C. Daran, and F. Secheresse, *J. Chem. Soc., Dalton Trans.*, **1994**, 1311.
4) Di-μ-Se complexes were reported recently. M. Nasreldin, G. Henkel, G. Kampmann, B. Krebs, G. J. Lamprecht, C. A. Routledge, and A. G. Sykes, *J. Chem. Soc., Dalton Trans.*, **1993**, 737.
5) B. Spivack and Z. Dori, *J. Chem. Soc., Dalton Trans.*, **1973**, 1173.
6) S. Khalil, B. Sheldrick, A. B. Soares, and A. G. Sykes, *Inorg. Chim. Acta*, **25**, L83 (1977).
7) S. Khalil and B. Sheldrick, *Acta Crystallogr., Sect. B: Struct. Crystallogr. Cryst. Chem.*, **B34**, 3751 (1978).
8) A. Kojima, S. Ooi, Y. Sasaki, K. Z. Suzuki, K. Saito,

and H. Kuroya, *Bull. Chem. Soc. Jpn.*, **54**, 2457 (1981).
9) S. Ikari, Y. Sasaki, and T. Ito, *Inorg. Chem.*, **28**, 447 (1989).
10) S. Ikari, Y. Sasaki, A. Nagasawa, C. Kabuto, and T. Ito, *Inorg. Chem.*, **28**, 1248 (1989).
11) S. Ikari, Y. Sasaki, and T. Ito, *Inorg. Chem.*, **29**, 53 (1990).
12) M. Yamazaki and T. Shibahara, *Inorg. Chim. Acta*, **205**, 45 (1993).
13) a) G. G. Kneale, A. J. Geddes, Y. Sasaki, T. Shibahara, and A. G. Sykes, *J. Chem. Soc., Chem. Commun.*, **1975**, 356; b) G. G. Kneale and A. J. Geddes, *Acta Crystallogr., Sect. B*, **B31**, 1233 (1975).
14) T. Shibahara, B. Sheldrick, and A. G. Sykes, *J. Chem. Soc., Chem. Commun.*, **1976**, 523.
15) T. Shibahara, H. Kuroya, K. Matsumoto, and S. Ooi, *J. Am. Chem. Soc.*, **106**, 789 (1984).
16) T. Shibahara, H. Kuroya, K. Matsumoto, and S. Ooi, *Inorg. Chim. Acta*, **116**, L25 (1986).
17) T. Shibahara, H. Kuroya, H. Akashi, K. Matsumoto, and S. Ooi, *Inorg. Chim. Acta*, **212**, 251 (1993).
18) H. Burgi, G. Anderegg, and P. Blauenstein, *Inorg. Chem.*, **20**, 3829 (1981).
19) S. Ikari, T. Ito, W. McFarlane, M. Nasreldin, B. -L. Ooi, Y. Sasaki, and A. G. Sykes, *J. Chem. Soc., Dalton Trans*, **1993**, 2621.
20) H. Toftlund and S. Yde-Andersen, *Acta Chem. Scand., Ser. A*, **A35**, 575 (1981).
21) S. Ikari, K. Kobayashi, Y. Sasaki, and T. Ito, unpublished result.
22) A. Neves, K. Wieghardt, B. Nuber, and J. Weiss, *Inorg. Chim. Acta*, **150**, 183 (1988).
23) H. Toftlund, O. Simonsen, and E. Pedersen, *Acta Chem. Scand.*, **44**, 676 (1990).
24) S. Pal, J. W. Gohdes, W. C. A. Wilisch, and W. H. Armstrong, *Inorg. Chem.*, **31**, 713 (1992).
25) K. Z. Suzuki, Y. Sasaki, S. Ooi, and K. Saito, *Bull. Chem. Soc. Jpn.*, **53**, 1288 (1980).
26) G. L. Blackmer, K. J. Johnson, and R. L. Roberts, *Inorg. Chem.*, **15**, 596 (1976).
27) J. B. Mandel, C. Maricondi, and B. E. Douglas, *Inorg. Chem.*, **27**, 2990 (1988).
28) Y. Sasaki, R. S. Taylor, and A. G. Sykes, *J. Chem. Soc., Dalton Trans.*, **1975**, 396.
29) The chemical formula of this compound is still uncertain. Since, a pure sample of this complex was difficult to obtain, crude salt was used as a starting material for the preparation of the new W complexes. O. Collenberg, *Z. Anorg. Allg. Chem.*, **102**, 247 (1918).
30) J. Sandström, "Dynamic NMR Spectroscopy," Academic Press, New York (1982).
31) "International Tables for X-Ray Crystallography," Kynoch, Birmingham, England (1974).
32) T. Sakurai and K. Kobayashi, *Rikagaku Kenkyuusho Hokoku* (*Rep. Inst. Phys. Chem. Res.*), **55**, 69 (1979).
33) C. K. Johnson, "ORTEP II. Report ORTL-5138," Oak Ridge National Laboratory, Oak Ridge, TN (1976).
34) A. T. McPhail, *J. Chem. Soc., Dalton Trans.*, **1977**, 1202.
35) a) A. E. Merbach, *Pure Appl. Chem.*, **54**, 1479 (1982); b) A. E. Merbach, *Pure Appl. Chem.*, **59**, 161 (1987).
36) T. W. Swaddle, *Adv. Inorg. Bioinorg. Mech.*, **2**, 96 (1983).
37) K. Unoura, T. Ooi, K. Tanaka, and A. Iwase, *J. Electroanal. Chem.*, **252**, 335 (1988).
38) F. A. Schultz and D. T. Sawyer, *J. Electroanal. Chem.*, **17**, 207 (1968).
39) V. R. Ott and F. A. Schultz, *J. Electroanal. Chem.*, **59**, 47 (1975).
40) V. R. Ott, D. S. Swieter, and F. A. Schultz, *Inorg. Chem.*, **16**, 2538 (1977).
41) T. Fukumoto, A. Kikuchi, K. Umakoshi, and Y. Sasaki, unpublished.
42) D. H. Brown, P. G. Perkins, and J. J. Stewart, *J. Chem. Soc., Dalton Trans.*, **1972**, 1105.
43) B. Jezowska-Trzebiatowska, T. Glowiak, M. F. Rudolf, M. Sabat, and J. Sabat, *Russ. J. Inorg. Chem.*, **22**, 1590 (1977).
44) J. D. Rush and B. H. J. Bielski, *Inorg. Chem.*, **24**, 3895 (1985).
45) N. S. Hush, *Prog. Inorg. Chem.*, **8**, 391 (1967).
46) M. B. Robin and P. Day, *Adv. Inorg. Chem. Radiochem.*, **10**, 247 (1967).